2014 IEEE International Conference on Robotics & Automation (ICRA)
Hong Kong Convention and Exhibition Center
May 31 - June 7, 2014. Hong Kong, China

# A Novel Two-dimensional Locomotion Scheme of a Micro-robot with Only a Uniform Magnetic Field

Jinsoo Kim and Seung-Jong Kim

*Abstract*— **This paper presents a novel motion control method of a micro-robot for biomedical applications. The proposed micro-robot is composed of a permanent magnet with oblique magnetization, and the electromagnetic actuation (EMA) system consists of only two pairs of Helmholtz coils arranged at a right angle on a horizontal plane. While conventional systems generally use the magnetic field gradient for the propulsion, the proposed system uses only a uniform magnetic field. By virtue of these strategies, we can make the system smaller and reduce the power consumption compared to the pre-existing EMA systems. To verify the feasibility of the proposed system, basic experiments and trajectory tracking were performed under different environments.**

## I. Introduction

Because of the size limitation of the micro-robot, the self-propulsion type micro-robot which has the actuation module including the power source is not suitable for biological or medical applications. To overcome such disadvantages, different kinds of actuation mechanisms have been proposed to propel the micro-robot with a wireless energy source. Among several actuation methods, an electromagnetic actuation (EMA) system composed of Helmholtz coils and Maxwell coils has been in the spotlight due to its simplicity. For example, K. B. Yesin et al. [1] suggested a two-dimensional EMA system with a motor, a Helmholtz pair, and a Maxwell pair. This initial system showed the possibility of the EMA system to control the micro-robot. However, its use in medical applications is limited because of its large size, mechanical moving part, and high power consumption. Since then, several variations have been researched to solve the aforementioned problems. Two-dimensional EMA systems with relatively reduced power [2-5], a micro-robot for drilling [6], and an EMA system with a clamping coil [7] were presented. Furthermore, there were also various attempts to implement an EMA system for three-dimensional motion control [8-11]. Especially, B. J. Nelson et al. showed fairly good results of a three-dimensional EMA system entitled 'OctoMag' for the purpose of intraocular surgery [12-15]. After targeting the size of a workspace to be $2\times2\times2$ ($mm^3$), they used the large size of soft-magnetic-core electromagnets to generate accurate and high magnetic fields.

*This research was supported by the Korea Institute of Science and Technology (KIST) Institutional Program (Project no.2E24721).

Jinsoo Kim is now with Center for Bionics, Korea Institute of Science and Technology (KIST), Hwarangno 14-gil 5, Seongbuk-gu, Seoul 136-791, Republic of Korea (cskarisma@kist.re.kr).

Seung-Jong Kim is also now with Center for Bionics, KIST (corresponding author, phone: +82-10-9229-3475; fax: +82-2-958-6784; e-mail: sjongkim@kist.re.kr, sjkim386@gmail.com).

However, all these previous methods used magnetic field gradients for generating thrust forces, and they required still too much power for propelling the micro-robot. To be specific, driving forces induced by the magnetic field gradient are directly proportional to the volume of the micro-robot, whereas the friction force at high Reynolds number is in proportion to the cross sectional area of it. In the case of very low Reynolds number less than 1, the Stokes' drag force is directly proportional to the characteristic linear dimension of the micro-robot. In other words, the smaller the micro-robot's size is, the greater the magnetic field gradient is needed. Thus, the power consumption problem becomes more aggravated. In order to avoid a usage of the magnetic field gradient, there was also different approach using the uniform magnetic field only. A micro-swimmer composed of a larger polystyrene bead and a smaller magnetic particle connected via a bacteria flagella filament was presented [16]. However, bacteria flagella may be dangerous for medical applications, and there is no evidence that inserting bacteria flagella into the human body will not incur any troubles.

In this paper, we propose a novel concept of EMA system for a micro-robot's two-dimensional motion control without using a magnetic field gradient. Different from previous works, the proposed EMA system requires only one stationary Helmholtz pair of each x- and y-axis, respectively. By virtue of removing an additional coil pair and utilizing nothing but a uniform magnetic field, the newly proposed EMA system can have a smaller volume and lower power consumption than the previous ones. Furthermore, these advantages will be amplified for the smaller size of the micro-robot. In our study, we introduce the postulates of electromagnetic theory in section Ⅱ. Section Ⅲ gives a detail explanation of the micro-robot and our proposed EMA system. Section Ⅳ deals with two different principles of generating thrust force. Next, section Ⅴ presents the experiment results and section Ⅵ gives the discussions. Lastly, section Ⅶ concludes the research of the paper.

## II. Postulates of Electromagnetic Theory

When a magnetic moment is placed in an externally produced magnetic field, it has a potential energy. As a result, the external magnetic field can apply both magnetic torque and force to it. In other words, there exists aligning torque on the micro-robot which has the magnetic moment, as follows:

$$\boldsymbol{\tau} = V\mathbf{M}\times\mathbf{B} \tag{1}$$

where $V$ and $\mathbf{M}$ are the volume and magnetization of a micro-robot, and $\mathbf{B}$ represents an externally applied magnetic field.

If the external magnetic field is non-uniform, there will be a magnetic force proportional to the magnetic field gradient [17]. It can be described as:

$$\mathbf{F} = V(\mathbf{M}\cdot\nabla)\mathbf{B} \tag{2}$$

A pair of Helmholtz coils consists of two identical circular coils that are placed symmetrically along a common axis and separated by a distance equal to the radius of the coil. Each coil carries an equal current flowing in the same direction, and this makes it possible to generate a uniform magnetic field [18]. Thus, two pairs of Helmholtz coils are used to align the micro-robot on a plane by generating a uniform magnetic field in a desired direction. The micro-robot experiences magnetic torque until its orientation coincides with the direction of the magnetic field, and it is not affected by the magnetic force by virtue of the uniform magnetic field. The magnetic field at the center of workspace is obtained as:

$$B_x(x=0) = \left(\frac{4}{5}\right)^{1.5}\frac{\mu_0 n_x i_x}{R_x} \tag{3}$$

where $\mu_0$, $n_x$, $i_x$, $R_x$ are the magnetic permeability of free space, the number of coil turns, the current intensity of each coil, and the radius of coil, respectively. The subscript $x$ means the $x$ direction.

Even though Helmholtz coils produce a uniform magnetic field, if the workspace is set too large, then there may be unintended consequences. For instance, when the micro-robot is positioned at the end of the workspace, it will experience a force due to the magnetic field gradients. Therefore, the boundary of the workspace is decided to $\left(x, y = \pm\frac{1}{6}R_x\right)$. Helmholtz configuration has only a 0.09% variation in field strength between the center and the boundary of a workspace. The magnetic field at the boundary of a workspace is calculated as:

$$B_x\big|_{x=\frac{1}{6}R_x} = \frac{1}{2}\left\{\left(\frac{9}{10}\right)^{1.5} + \left(\frac{9}{13}\right)^{1.5}\right\}\frac{\mu_0 n_x i_x}{R_x} \tag{4}$$

## III. Micro-robot and EMA Control System

### A. Configuration of EMA coils

The proposed EMA system consists of two sets of circular shaped Helmholtz coils which are perpendicularly arranged as shown in Fig. 1. In the figure, the X-axis coils are called HX1 and HX2, and the Y-axis coils are referred to as HY1 and HY2. Table I shows the specifications of the coils. The diameter of the used cooper wire is 1($mm$) and the workspace of the micro-robot is set to $20\times20$ ($mm^2$) that is a ninth of the area enclosed by EMA coils. In addition, the EMA system is made of the duralumin to avoid the magnetization by an external magnetic field. With these specifications, the X-directional maximum magnetic field at the center of the workspace is calculated at 10.62($mT$) with a current of 5($A$) (the maximum current our power amplifier can provide) applied to HX1 and HX2 in the same direction. Here, note that these currents are directly proportional to the magnetic torque. In the case of the Y direction, the maximum magnetic field is 7.74($mT$), which is sufficiently high to control the direction of the micro-robot.

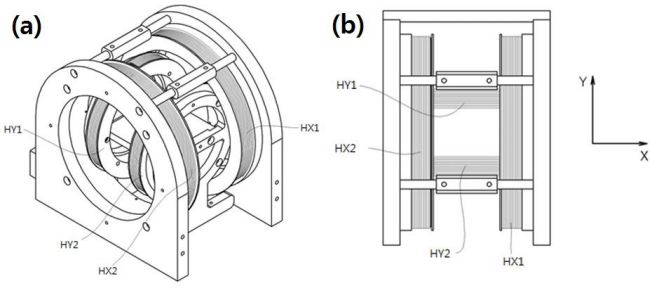


Figure 1 (a) A 3D design drawing (b) A top view of the EMA coils

TABLE I. Specificaions of Each EMA Coils

| Type of coil | Radius (mm) | Number of turns | Width of bobbin (mm) | Height of bobbin (mm) |
|---|---|---|---|---|
| HX1, HX2 | 80 | 189 | 18 | 14 |
| HY1, HY2 | 60 | 104 | 14 | 10 |

### B. Oscillatory magnetic field

In order to generate an oscillatory magnetic field, two parameters are required, e.g. base angle ($\theta_b$) and perturbation angle ($\theta_p$). The direction of an oscillatory magnetic field is represented as:

$$\theta(t) = \theta_b + \theta_p\cos(\omega t) \tag{5}$$

where $\omega$ denotes the angular velocity. Fig. 2 shows the case of $\theta_b = 45^\circ$, $\theta_p = 30^\circ$.

The Helmholtz coil pairs can generate an oscillatory magnetic field using a trigonometric function form of currents. For example, the currents of Helmholtz coil pairs can be assigned as:

$$i_x(t) = \alpha\frac{R_x}{n_x}\cos\left(\theta_b + \theta_p\cos(\omega t)\right) \tag{6}$$

$$i_y(t) = \alpha\frac{R_y}{n_y}\sin\left(\theta_b + \theta_p\cos(\omega t)\right) \tag{7}$$

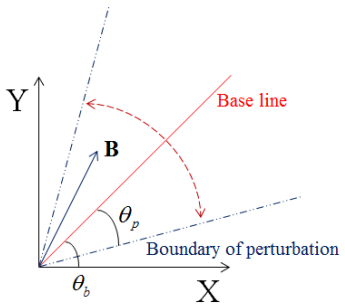


Figure 2 Oscillatory magnetic field

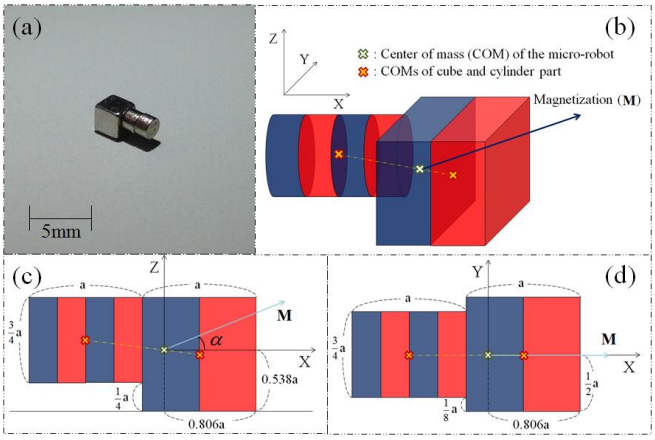


Figure 3 (a) A photo of the micro-robot (b) The magnetization direction of the micro-robot in 3D view (c) Vector **M** in a top view (d) Vector **M** in a side view (The yellow mark 'X' at the origin in figure (c) and (d) represents the center of mass (COM) of the micro-robot. The orange marks 'X' in figure (c) and (d) represent the COM of the cube and cylinder part.)

where $i_x(t)$ and $i_y(t)$ denote the currents of x-axis and y-axis Helmholtz coil pairs respectively, and $\alpha$ is a proportionality constant.

The magnetization of the micro-robot should coincide with the generated oscillating magnetic field. In spite of its uniform distribution, it can also have an effect on the micro-robot's translational motion. To be specific, the direction of the propulsion motion is also determined by the base angle of the oscillating magnetic field.

### C. *Magnetization and shape of the micro-robot*

The presented micro-robot is composed of the neodymium permanent magnets ( $B_r = 1.22(T)$ , $H_c = 891(kA/m)$ , NdFe35). Two cylinder-type magnets which have the diameter of 1.5 (mm) and the thickness of 1 (mm) are attached to a cube type magnet ( $2\times2\times2(mm^3)$ ) as shown in Fig. 3.

Our proposed EMA system is designed to generate a uniform magnetic field which is directly related to magnetic torque; the magnetic torque itself cannot propel the micro-robot. In the case of generating thrust force without a magnetic field gradient, it is required to make nonzero net friction force. Strictly speaking, the time average of net friction force should have directionality based on the base angle of an oscillatory magnetic field. Furthermore, it is the magnetization direction of the micro-robot that plays an important role in generating that directionality. Thus, the micro-robot is magnetized obliquely, and the angle between the x axis and the magnetization direction in Fig. 3 (c) is referred to as the oblique angle ( $\alpha$ ). A detailed explanation will be described in Section Ⅳ.

### D. *Composition of overall EMA control system*

The entire EMA system consists of a micro-robot, a localization system, a control part, a power amplifier, and the EMA coils. A localization system (e.g. industrial camera) detects the micro-robot's position and orientation, while the control part calculates exact currents based on the feedback

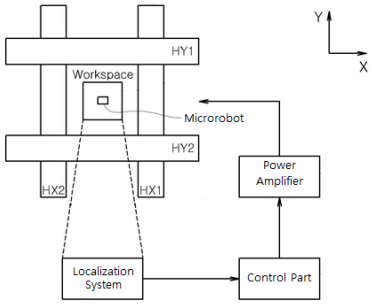


Figure 4 A schematic diagram of the whole system

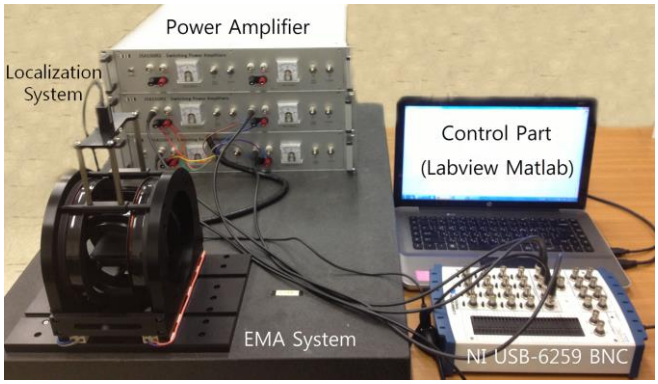


Figure 5 Overall view of the EMA control system

data. A power amplifier applies a current to make the pre-calculated magnetic field distribution and the micro-robot reacts to the magnetic field as described in Fig. 4.

To identify the direction and position of the micro-robot, a webcam (ARTCAM-022MINI, $752\times480$ , 50FPS) captures its image. Localization is performed using the Matlab program, by comparing the image and the background image pre-captured without the micro-robot. The system also includes a NI USB-6259 device for data transfer, a power amplifier (PWM type, $-5\sim5(A)$ , bandwidth 100(Hz)) for the voltage-to-current signal conversion, and the Labview program for the real-time control of the micro-robot. Fig. 5 shows the overall EMA control system.

## IV. Principle of Propelling the Micro-robot by Using only Uniform Magnetic Fields

### A. *Moving forward*

When the uniform magnetic field is applied in an x-y plane, the micro-robot rotates around its center of mass (COM) to align its magnetization with the external magnetic field. Magnetic torque can be decomposed into the z component and the x-y component as noted in (8).

$$\boldsymbol{\tau} = V\mathbf{M}\times\mathbf{B} = V\left(\mathbf{M}_{\perp z}+\mathbf{M}_z\right)\times\mathbf{B} = V\mathbf{M}_{\perp z}\times\mathbf{B}+V\mathbf{M}_z\times\mathbf{B} \quad (8)$$

where $\mathbf{M}_{\perp z}$ and $\mathbf{M}_z$ represent the x-y component and the z component of magnetization, respectively.

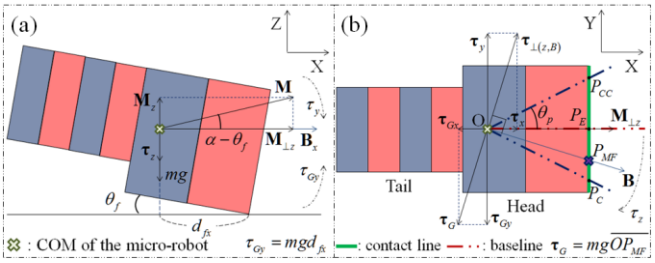


Figure 6 Vector analysis of moving forward in (a) x-z plane (b) x-y plane during the clockwise rotation (COM is referred to as point O. The green solid line in (b) represents the contact points between the micro-robot and surface. The red dashed line and blue dashed lines in (b) are the baseline and the boundary of perturbation, respectively. $P_C$ and $P_{CC}$ represent the intersection points between the boundary of perturbation and contact line. $P_E$ is the intersection point between the base line and the contact line. $P_{MF}$ is the intersection point between the magnetic field $\mathbf{B}$ and the contact line. $m$, $g$, $\boldsymbol{\tau}_x$, $\boldsymbol{\tau}_y$, $\boldsymbol{\tau}_{Gx}$, $\boldsymbol{\tau}_{Gy}$ are the micro-robot's mass, the acceleration of gravity, the x and y component of $\boldsymbol{\tau}_{\perp(z,B)}$, the x and y component of $\boldsymbol{\tau}_G$, respectively.)

The former term, $V\mathbf{M}_{\perp z}\times\mathbf{B}$, on the right hand side in (8) is called the z-axis magnetic torque ($\boldsymbol{\tau}_z$) which makes a clockwise or counterclockwise rotation in the x-y plane. The latter, $V\mathbf{M}_z\times\mathbf{B}$, is referred to as the x-y plane magnetic torque ($\boldsymbol{\tau}_{\perp(z,B)}$) that is orthogonal to the z axis and the magnetic field as illustrated in Fig. 6 (b). Furthermore, $\boldsymbol{\tau}_{\perp(z,B)}$ plays a significant role in changing the center of rotation (COR) (when the micro-robot rotates in x-y plane), which makes it possible to propel the micro-robot without the magnetic field gradient. When the tail part of the micro-robot is lifted because of the x-y plane magnetic torque ($\boldsymbol{\tau}_{\perp(z,B)}$), gravity makes gravitational torque ($\boldsymbol{\tau}_G$) in the opposite direction as described in Fig. 6. As a result of equilibrium of torques ($\boldsymbol{\tau}_{\perp(z,B)}=\boldsymbol{\tau}_G$), the micro-robot stands at a tilt angle ($\theta_f$), and it still has the z component of magnetization.

The x-y plane magnetic torque ($\boldsymbol{\tau}_{\perp(z,B)}$) presses on the maximum friction point $P_{MF}$ the most, and therefore this point receives the highest friction and functions like a hinge. To be specific, because of this unsymmetrical friction, the center of rotation is changed from the point O to the point on the line segment $\overline{OP_{MF}}$.

As described in Section Ⅲ, an oscillatory magnetic field is applied between the boundary of perturbation. In the case of clockwise rotation, $P_{MF}$ is located on the line segment $\overline{P_EP_C}$, whereas it is located on the line segment $\overline{P_EP_{CC}}$ during the counterclockwise rotation. The time average of the net friction force has the directionality which is the same with the base angle. As a result, a gradual change of the center of rotation can make it possible for the micro-robot to move forward with a crawling type of motion.

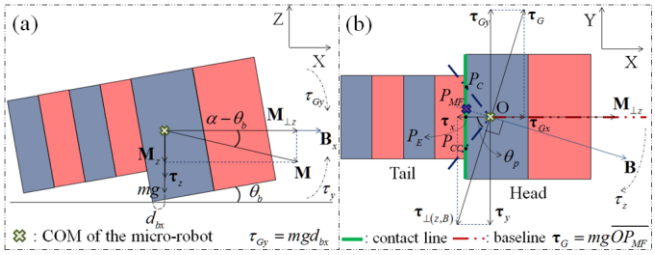


Figure 7 Vector analysis of backward movement in (a) x-z plane (b) x-y plane during clockwise rotation ($\theta_b$ is the tilt angle.)

### B. *Moving backwards*

The micro-robot can be moved in any direction by the forward-moving scheme explained before. One interesting fact is that if the micro-robot is initially magnetized with the oblique magnetic field which has a negative z component as illustrated in Fig. 7 (a), it moves backwards in spite of applying the same oscillatory magnetic field.

The moving principle is similar to the previous one, except for several things. The direction of the x-y plane magnetic torque ($\boldsymbol{\tau}_{\perp(z,B)}$) is changed as a consequence of the negative z component of magnetization, and the contact line is changed to the cylinder side as shown in Fig. 7. Also, $P_{MF}$ is located on the line segment $\overline{P_EP_C}$ during clockwise rotation, whereas it is located on the line segment $\overline{P_EP_{CC}}$ during the counterclockwise rotation as described in Fig. 7 (b). Thus, in this case, the gradual change of center of rotation makes the micro-robot move backwards.

### C. *The role of the tail*

According to the explanation in Section Ⅳ A. and B., it is possible to move the micro-robot without the tail part in the forward or backward direction. The only difference between the previous proposed structure and the micro-robot without a tail is the location of COM. However, when it comes to rotation around COR which does not coincide with COM, the tail part enhances the inertial effects and this makes the micro-robot move faster. In moving backwards, this effect is slightly scaled down because biased COM shortens the length of $\overline{OP_{MF}}$, reduces x-y plane magnetic torque ($\boldsymbol{\tau}_{\perp(z,B)}$) and tilt angle ($\theta_b$), and lessens the shift of COR from COM. If the tail is detached, the COM is located at the exact center of the cube component and moving speed of the micro-robot during both forward and backward motion is almost the same.

## V. Experiment Results

First, we confirmed the validity of moving forward and backward strategy with and without the tail structure. During all these experiments, each parameter was set to the same value; for example, the frequency of oscillating field ($f=\dfrac{\omega}{2\pi}$) and perturbation angle were set to 1.25(Hz) and $30^\circ$, respectively. Open-loop actuation tests based on the

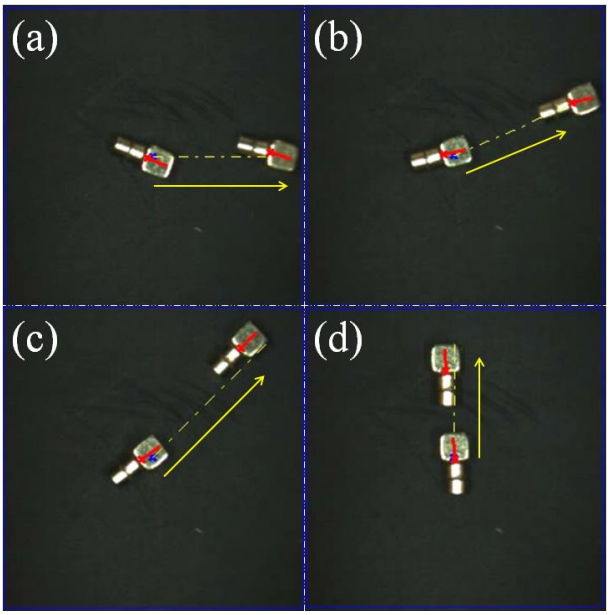


Figure 8 Forward motion with the tail for various base angles (a) $\theta_b = 0^\circ$ (b) $\theta_b = 22.5^\circ$ (c) $\theta_b = 45^\circ$ (d) $\theta_b = 90^\circ$ (Two frames from a movie are superimposed with the path taken by the robot. The yellow arrow shows the desired moving direction ( $\theta_b$ ). The red mark 'x' and line represent the real-time localization results, i.e. position and orientation of the micro-robot, by using a detection algorithm. The blue mark 'x' represents the center of workspace.)

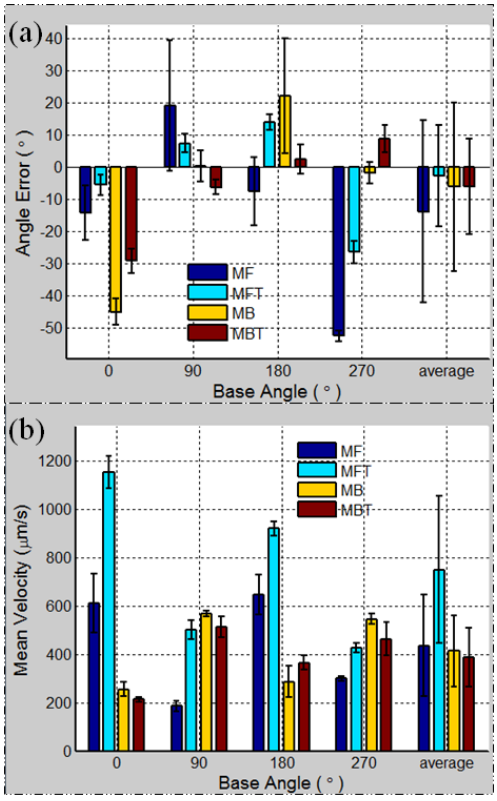


Figure 9 (a) Error between the base angle (expected moving angle) and the actual moving angle (b) Mean velocity for each direction

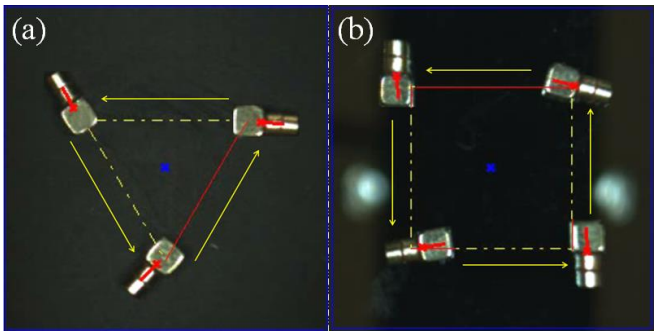


Figure 10 (a) Triangular trajectory tracking on a slightly uneven surface (b) Square trajectory tracking on a very smooth surface (Several frames from a movie are superimposed with the path taken by the robot, shown with the yellow arrows. The real-time position and orientation of the micro-robot is marked with a red line and the center of workspace is represented by the blue mark 'x'.)

proposed methods were verified successfully by generating thrust force of various angles as depicted in Fig. 8.

However, there were also angle errors and velocity fluctuations depending on the base angle and the type of methodology. We measured the errors and fluctuations, and calculated the mean and standard deviation as illustrated in Fig. 9. 'MF' and 'MB' mean 'Moving Forward' and 'Moving Backwards', and the letter 'T' represents an acronym for 'Tail'. Thus, 'MF' is the case of moving forward without the tail part, whereas 'MFT' is the case of moving forward with the tail. Each trial classified with the both angles ( $0^\circ$, $90^\circ$, $180^\circ$, and $270^\circ$ ) and the types of method (MF, MFT, MB, and MBT) were repeated at least 5 times.

Lastly, we carried out the trajectory tracking based on the prior direction test and localization data. Different shapes of trajectory were tried and we verified reliable results in Fig. 10. Different types of surface were also attempted in order to identify the role of friction affected by surface roughness. Fig. 10 (a) was performed on a duralumin surface which was slightly uneven on a microscopic level, whereas (b) was done on a very smooth silicon wafer surface whose roughness was manufactured with nanoscale precision. All these experiments are available in the supplementary video clips.

## VI. DISCUSSION

Our proposed moving mechanisms are supported by the experiment data. In Fig. 9 (b), MFT has greater mean velocity than MF by virtue of increasing inertial effects as we described in section Ⅳ. MF and MB have almost the same velocity, because both of them do not have a tail, and thus there is no difference between them except for the moving direction. Of course, each velocity shows different tendencies depending on the base angle, but we deal with the average case only. In the case of MBT, the increased inertial effect is counterbalanced by the reduction of distance between COM and COR, so its mean velocity is similar to MF and MB. In sum, MFT has the greatest mean velocity with the lowest angle error among these methods, and this is why we choose MFT for trajectory tracking in Fig. 10.

In the case of trajectory tracking, we performed several experiments on different surfaces. When the tracking is performed on a very flat surface, mean velocity is reduced compared to the velocity of an uneven surface, because the friction coefficient of a flat silicon wafer is smaller than that of the uneven case. As a result, the reduction in friction force leads to a smaller distance between COM and COR, and causes a lower moving velocity of the micro-robot. Thus, these results indicate that friction plays a significant role on the thrust force.

Finally, we checked the execution time of trajectory tracking between the proposed method and previous approaches using the magnetic field gradient in [1-11, 15]. All environment conditions (e.g. the shape and overall distance of trajectory, the size and shape of the micro-robot, and the roughness of surface) are set to the same value. The execution time of our proposed method is almost equal to that of previous research, even though our method requires only a small amount of the current in comparison to the previous ones. In other words, the proposed method is power efficient for two-dimensional motion control of the micro-robot.

## VII. Conclusion

In this paper, we suggested a new type of micro-robot with oblique magnetization and proposed a novel scheme of micro-robot's two-dimensional motion control without magnetic field gradient generally used by conventional approaches. Motion control with only a uniform magnetic field can make it possible to control the micro-robot in a fairly accurate way and reduce the power consumption compared to the previous methods.

In order to apply our proposed method to the medical field, it should be verified that our method can make the sufficient thrust force to overcome the viscous drag forces in the body. Furthermore, it might be possible to utilize the viscous drag synergistically. These considerations including fluidic environment are also consequential in the context of applicability at low Reynolds number in order to minimize the size of the micro-robot. Furthermore, three-dimensional extension of the proposed method will be required to increase the application field.

## Appendix

Supplementary video clips associated with this paper can be found in the online version.

## Acknowledgment

This research was supported by the Korea Institute of Science and Technology (KIST) Institutional Program (Project no.2E24721).

## References

[1] K. B. Yesin, K. Vollmers, and B. J. Nelson, "Modeling and control of untethered biomicrorobots in a fluidic environment using electromagnetic fields," *Int. J. Robot. Res.*, vol. 25, no. 5-6, May-June 2006.

[2] H. Choi, J. Choi, G. Jang, J. o. Park, and S. Park, "Two-dimensional actuation of a microrobot with a stationary two-pair coil system," *Smart Mater. Struct.*, vol. 18, no. 5, May 2009.

[3] S. Jeon, G. Jang, H. Choi, and S. Park, "Magnetic navigation system with gradient and uniform saddle coils for the wireless manipulation of micro-robots in human blood vessels," *IEEE Trans. Magn.*, vol. 46, no. 6, June 2010.

[4] H. Choi, J. Choi, S. Jeong, C. Yu, J. o. Park, and S. Park, "Two-dimensional locomotion of a microrobot with a novel stationary electromagnetic actuation system," *Smart Mater. Struct.*, vol.18, no. 11, Nov. 2009.

[5] Q. Cao, X. Han, B. Zhang, and L. Li, "Analysis and optimal design of magnetic navigation system using Helmholtz and Maxwell coils," *IEEE Trans. Appl. Supercon.*, vol. 22, no. 3, June 2012.

[6] S. Jeong, H. Choi, K. Cha, J. Li, J. o. Park, S. Park, "Enhanced locomotive and drilling microrobot using precessional and gradient magnetic field," *Sensor. Actuat. A-Phys.*, vol. 171, pp. 429-435, Nov. 2011.

[7] S. Floyd, C. Pawashe, and M. Sitti, "An untethered magnetically actuated micro-robot capable of motion on arbitrary surfaces," *IEEE Int. Conf. on Robotics and Automation*, pp. 419-424, May 2008.

[8] S. Jeong, H. Choi, J. Choi, C. Yu, J. o. Park, and S. Park, "Novel electromagnetic actuation (EMA) method for 3-dimensional locomotion of intravascular microrobot," *Sensor. Actuat. A-Phys.*, vol. 157, pp. 118-125, Jan. 2010.

[9] C. Yu, H. Choi, J. Park, and S. Park, "Three-dimensional electromagnetic actuation system for intravascular locomotion," IEEE/RSJ Int. Conf. on Intelligent Robots and Systems, pp. 540-545, Oct. 2009.

[10] H. Choi, K. Cha, J. Choi, S. Jeong, S. Jeon, G. Jang, J. o. Park, and S. Park, "EMA system with gradient and uniform saddle coils for 3D locomotion of microrobot," *Sensor. Actuat. A-Phys.*, vol. 163, Sep. 2010.

[11] C. Yu, J. Kim, H. Choi, J. Choi, S. Jeong, K. Cha, J. o. Park, and S. Park, "Novel electromagnetic actuation system for three-dimensional locomotion and drilling of intravascular microrobot," *Sensor. Actuat. A-Phys.*, vol. 161, pp. 297-304, June 2010.

[12] J. J. Abbott, O. Ergeneman, M. P. Kummer, A. M. Hirt, and B. J. Nelson, "Modeling magnetic torque and force for controlled manipulation of soft-magnetic bodies," *IEEE Trans. on Robotics*, vol. 23, no. 6, Dec. 2007.

[13] Z. Nagy, O. Ergeneman, J. J. Abbott, M. Hutter, A. M. Hirt, and B. J. Nelson, "Modeling assembled-MEMS microrobots for wireless magnetic control," *IEEE Int. Conf. on Robotics and Automation*, pp. 874-879, May 2008.

[14] C. Bergeles, K. Shamaei, J. J. Abbott, and B. J. Nelson, "Single-camera focus-based localization of intraocular devices," *IEEE Trans. on Biomed. Eng.*, vol. 57, no. 8, Aug. 2010.

[15] M. P. Kummer, J. J. Abbott, B. E. Kratochvil, R. Borer, A. Sengul, and B. J. Nelson, "OctoMag: an electromagnetic system for 5-DOF wireless micromanipulation," *IEEE Trans on Robotics*, vol. 26, no. 6, Dec. 2010.

[16] U. K. Cheang, D. Roy, J. H. Lee, and M. J. Kim, "Fabrication and magnetic control of bacteria-inspired robotic microswimmers," *Appl. Phys. Lett.*, vol. 97, Issue 21, Nov. 2010.

[17] T. H. Boyer, "The force on a magnetic dipole," *Am. J. Phys.*, vol. 56, no. 8, Aug. 1988.

[18] S. T. Lin and A. R. Kaufmann, "Helmholtz coils for production of powerful and uniform fields and Gradients," *Reviews of Modern Phys.*, vol. 25, no. 1, Jan. 1953.